NJC

New Journal of Chemistry

A journal for new directions in chemistry

Accepted Manuscript

This article can be cited before page numbers have been issued, to do this please use: F. Carmona Viglianco, J. D. Zaragoza Puchol, O. Parravicini, A. Garro, R. Enriz, G. Feresin, M. Kurina-Sanz and A. A. Orden, *New J. Chem.*, 2020, DOI: 10.1039/D0NJ00282H.

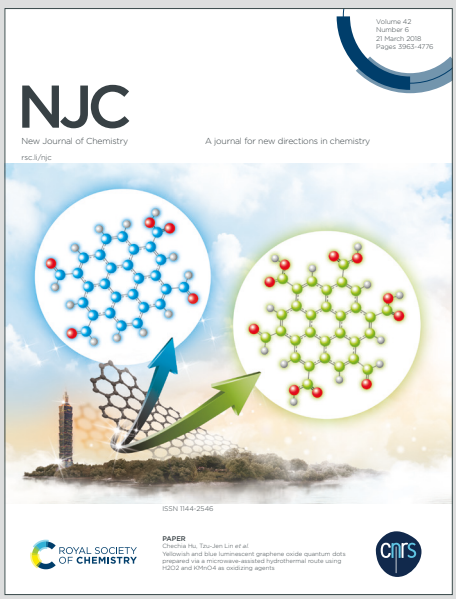

ROYAL SOCIETY OF CHEMISTRY

rsc.li/njc

View Article Online
DOI: 10.1039/D0NJ00282H

Synthesis, biological evaluation and molecular modeling studies of substituted *N*-benzyl-2-phenylethanamine as cholinesterase inhibitors

Florencia Carmona Viglianco[a], Daniel Zaragoza Puchol[b], Oscar Parravicini[c], Adriana Garro[c], Ricardo D. Enriz[c], Gabriela E. Feresin[b], Marcela Kurina-Sanz[a], Alejandro A. Orden[a]

[a] INTEQUI CONICET, Facultad de Química Bioquímica y Farmacia, Universidad Nacional de San Luis, Almirante Brown 1455, San Luis, D5700HHW, Argentina

[b] Instituto de Biotecnología, CONICET, Facultad de Ingeniería, Universidad Nacional de San Juan. Av. Libertador General San Martín 1109 (O), CP 5400, San Juan, Argentina

[c] IMIBIO-SL CONICET, Facultad de Química Bioquímica y Farmacia, Universidad Nacional de San Luis, Ejército de los Andes 950, San Luis, D5700HHW, Argentina

Corresponding author: E-mail aaorden@unsl.edu.ar

Abstract

In this work we report the synthesis of a series of derivatives of *N*-benzyl-2-phenylethanamine which is the framework of norbelladine, the natural common precursor of the Amaryllidaceae alkaloids. These compounds were assessed in the inhibition of both AChE and BChE which are the enzymes responsible for the breakdown of acetylcholine and hence they constitute targets in the palliative treatment of Alzheimer disease. In particular, brominated derivatives exhibited the lowest IC_{50} values against AChE. Interestingly, the presence of iodine in one of the aromatic rings highly increased the inhibition of BChE compared to its analogues, with an IC_{50} value similar to that of galantamine, which was the reference compound currently used in the treatment of AD. A possible mechanism of action for these compounds was determined by molecular modeling studies using combined techniques of docking and molecular dynamics simulations.

Keywords

Amaryllidaceae alkaloid precursor; AChE and BChE inhibition; norbelladine analogues; reductive amination; molecular modeling.

View Article Online
DOI: 10.1039/D0NJ00282H

Abbreviations

AD: Alzheimer Disease

ACh: acetylcholine

AChE: Acetylcholinesterase

BChE: Butyrylcholinesterase

IC_{50}: half maximal inhibitory concentration

Gal: Galantamine

MD: Molecular Dynamics

View Article Online
DOI: 10.1039/D0NJ00282H

1. Introduction

Alzheimer's disease (AD) is the most common type of dementia among older adults which is characterized by chronic neurodegenerative pathology that causes a significant and progressive functional disability, loss of cognition and altered behavior. Several factors have been described to play a role in the pathogenesis of AD including a deficit of acetylcholine (ACh), tau-protein aggregation and extracellular deposits of amyloid plaques. Consequently, multiple pharmacological targets can be tackled as a palliative treatment for this disease [1,2].

Cholinesterase inhibitors have been developed as therapeutic agents for AD based on the cholinergic dysfunction hypothesis which states that low levels of ACh lead to cognitive impairment and dementia [3]. The human brain contains two different cholinesterases: acetylcholinesterase (AChE; EC 3.1.1.7) and butyrylcholinesterase (BChE; EC 3.1.1.8) which are the enzymes responsible for hydrolyzing the neurotransmitter ACh into choline and acetate. Currently, only three AChE inhibitors have been approved by the FDA and used for the palliative treatment of mild to moderate symptoms of AD: galantamine, donepezil and rivastigmine. AChE has gained great relevance as a target for novel drug discovery because of its dual functionality: ACh hydrolysis and amyloid beta peptide aggregation [4]. On the other hand, BChE has a role in the hydrolysis of ACh but also non-enzymatic functions, such as being involved in anti-inflammatory pathways and delaying the rate of neurotoxic amyloid-β fibril formation [5] which foster the study of this enzyme as an important target in AD pharmacotherapy.

Several studies have been performed in order to discover novel anticholinesterases either as naturally-occurring compounds or synthetic inhibitors. Plant species and their potentially active compounds such as terpenes, coumarins, polyphenols and alkaloids have been screened for anti-AChE activity being the latter the most potent compounds assessed [6]. Recently, some molecules have been designed and synthesized based on different scaffolds such as chalcone-derivatives [7–9], 1,2,3-triazole-chromenone carboxamides [10], dibenzo-γ-pyrones [11], benzofurans [12], spirooxindoles [13], tacrine-ferulic acid and quinoline-ferulic acid hybrids as multi-target-directed ligands [14,15], among many others [2]. Most of them have shown moderate to significant cholinesterase inhibitory activity. Also, the modification of natural compounds by xenobiotic biotransformation has been a tool to increase their biological activity [16].

Norbelladine is an alkaloid-like amine (protoalkaloid) resulting from the condensation of 3,4-dihydroxybenzaldehyde -protocatechuic aldehyde- (derived from phenylalanine) and tyramine

View Article Online
DOI: 10.1039/D0NJ00282H

(derived from tyrosine). This is the common precursor in the biosynthesis of all Amaryllidaceae alkaloids which is further regioselectively methylated to give 4'-*O*-methylnorbelladine that can undergo three different types of oxidative phenol coupling reactions (*para-para'*, *ortho-para'*, *ortho'-para* couplings) to give alkaloids such as haemanthamine, lycorine and galantamine. The latter is primarily isolated from daffodil (*Narcissus* spp.), snowdrop (*Galanthus* spp.), and summer snowflake (*Leucojum aestivum*) and has been used in the palliative treatment of Alzheimer's disease in the early stages [17,18]. The potential health effects of the Amaryllidaceae alkaloids have been widely investigated [19] although there are a limited number of studies of the bioactivities of their precursors. One recent example is the antioxidant and anti-inflammatory effects of norbelladine via scavenging radicals and inhibiting both COX-1 and 2 enzymes [20].

Halogens in ligand–target complexes play an important role due to steric aspects that influence their conformation, allow intermolecular interactions that favorably contribute to the stability and also increase membrane permeability [21]. Although less abundant than fluorine-containing drugs which are estimated 20 % of all pharmaceuticals, there are interesting examples of commercially available organobromine drugs, such as the mucolytic drug bromhexine, the vasodilator nicergoline, the sedative and hypnotic brotizolam and non-steroidal anti-inflammatory for ophthalmic use bromfenac [22]. On the other hand, iodine is highly used in nuclear medicinal diagnostic techniques and there are a few examples of iodine-containing organic compounds such as iobenguane, a blocking agent for adrenergic neurons, I^{131} iodocholesterol with diagnostic imaging activity, 4'-iodo-4'-deoxydoxorubicin with antiamyloid activity and 4-iodopropofol, an alkylphenol derivative with anticonvulsant activity [23].

In the present study, inspired by the common precursor of Amaryllidaceae alkaloids, we synthesized a series of substituted *N*-benzyl-2-phenylethanamine based on the norbelladine structure as a scaffold. Most of the compounds bear a halogen atom on one of the aromatic rings. These compounds were assessed as cholinesterase inhibitors and a plausible mechanism of action was explained by molecular modeling studies using combined techniques such as docking calculations and molecular dynamics simulations. As a result, the possible stereo-electronic requirements for these ligands were also discussed regarding to their different affinities.

2. Results and discussion

2.1. Synthesis of norbelladine analogues

View Article Online
DOI: 10.1039/D0NJ00282H

N-benzyl-2-phenylethanamine (norbelladine framework) was used as a key unit to design new analogues with different substitution patterns mainly at the A-ring. 4'-*O*-methylnorbelladine and several non-natural analogues were synthesized by condensation of substituted aromatic aldehydes (**1**-**9**) and tyramine (**10**) or phenylethylamine (**11**) to form the Schiff base and further reduced with sodium borohydride. The reductive amination to obtain 4'-*O*-methylnorbelladine (**12**) has been already described in literature with different yields [24–27]. Several experiments were conducted to improve the isolated yields, especially using some Lewis acid catalysts, bases and dehydrating agent in the reaction mixture as well as different temperatures (data not shown). The best results were obtained at room temperature in methanol using anhydride sodium sulfate as a desiccant and triethylamine (TEA) or KOH as a base to increase the nucleophile strength of the primary amine giving the desired products. Most of the halogenated norbelladine analogues precipitated during the work-up procedure in the alkaline aqueous medium at their corresponding isoelectric point and thus were purified by filtration and simple recrystallization. However, to recover **12** after work-up, it was necessary to perform a partition with ethyl acetate. As a result, a library of ten synthetic analogues of norbelladine was obtained in yields ranging from 51-92 % with purity higher than 96 % determined by GC-FID or GC-MS. The halogenated compounds were synthesized from the corresponding aldehydes as starting materials.

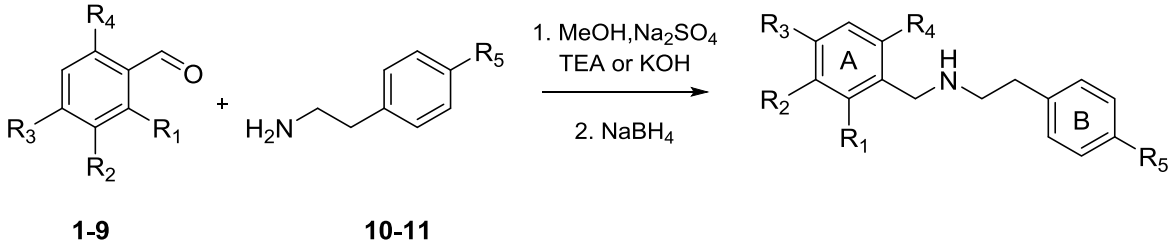

1-9 **10-11**

12	R^1: H	R^2: OH	R^3: OCH_3	R^4: H	R^5: OH
13	R^1: Cl	R^2: OH	R^3: OCH_3	R^4: H	R^5: OH
14	R^1: Br	R^2: OH	R^3: OCH_3	R^4: H	R^5: OH
15	R^1: I	R^2: OH	R^3: OCH_3	R^4: H	R^5: OH
16	R^1: H	R^2: OH	R^3: OCH_3	R^4: Br	R^5: OH
17	R^1: H	R^2: H	R^3: F	R^4: H	R^5: OH
18	R^1: H	R^2: H	R^3: Cl	R^4: H	R^5: OH
19	R^1: H	R^2: H	R^3: Br	R^4: H	R^5: OH
20	R^1: H	R^2: H	R^3: OH	R^4: H	R^5: OH
21	R^1: Br	R^2: OH	R^3: OCH_3	R^4: H	R^5: H

Fig. 1. Reductive amination for the synthesis of norbelladine analogues

View Article Online
DOI: 10.1039/D0NJ00282H

2.2. Cholinesterase inhibitory activity

The synthesized compounds were tested for cholinesterase inhibition of both *Electrophorus electricus* AChE and equine butyrylcholinesterase BChE according to Ellman's method [28] with some modifications [29], and the results were expressed as IC_{50} values. In order to make the compounds more water-soluble for the bioassays and avoid the use of co-solvents, the hydrochloride salts of **12**-**14** were prepared. No significant differences in the IC_{50} values for the inhibition of AChE or BChE were observed for the compounds with free amines compared to the amine salt (see Table S1).

Compounds **13**, **14**, **16** and **21** showed the lowest IC_{50} values for AChE inhibition. The introduction of halogenated substituents at the A-ring improved the cholinesterase inhibition compared to the natural compound 4'-*O*-methylnorbelladine (**12**) with the exception of iodine. Other authors have also discussed how the presence of halogens on thiophene chalcones and pyrazoline derivatives exerted an increase in the cholinesterase inhibition [7,8]. Brominated compounds on 2' position **14** and **21** were the most effective inhibitors against AChE exhibiting IC_{50} values of 16.79 ± 0.51 and 17.14 ± 3.17 μM, respectively, differing by one order of magnitude higher than the positive control galantamine (IC_{50} of Gal: 1.2 ± 0.1 μM). These studies suggest that the brominated derivatives of **12** show higher cholinesterase inhibition than their analogues, being good candidates to deepen for this bioactivity. On the other hand, monosubstituted derivatives (**17**-**20**) at the A-ring displayed no inhibition activity towards AChE. However, with the exception of the fluorinated compound **17**, they all showed to some extent some inhibition of BChE, being the brominated analogue the best inhibitor for this enzyme with an IC_{50} value of 23.90 ± 6.26.

Interestingly, when the OH group at the B-ring was not present (compound **21**) the product exerted a high inhibition of both cholinesterases with IC_{50} of 17.14 ± 3.17 for AChE and 13.35 ± 3.01 for BChE. This latter value was comparable to Gal (IC_{50} of 15.88 ± 1.6 μM). Also, compound **15** showed a high selectivity for BChE inhibition showing an IC_{50} value of 13.34 ± 2.79 μM.

View Article Online
DOI: 10.1039/D0NJ00282H

Table 1

Results of the cholinesterase inhibition with norbelladine analogues.

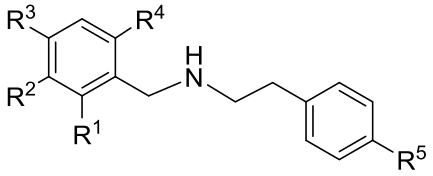

Compound	R^1	R^2	R^3	R^4	R^5	IC_{50} [μM] AChE	IC_{50} [μM] BChE	Selectivity to BChE
12	H	OH	OCH_3	H	OH	69.26±0.52	65.48±4.84	1.05
13	Cl	OH	OCH_3	H	OH	36.18±4.99	62.25±4.64	0.58
14	Br	OH	OCH_3	H	OH	16.79±0.51	49.91±3.01	0.34
15	I	OH	OCH_3	H	OH	173.66±14.78	13.34±2.79	13.01
16	H	OH	OCH_3	Br	OH	34.79±4.52	30.32±1.81	1.15
17	H	H	F	H	OH	>200	>200	n.d.
18	H	H	Cl	H	OH	>200	159.27±28.44	n.d.
19	H	H	Br	H	OH	>200	23.90±6.26	n.d.
20	H	H	OH	H	OH	>200	52.98±8.58	n.d.
21	Br	OH	OCH_3	H	H	17.14±3.17	13.35±3.01	1.28
Gal*						1.21±0.06	15.88±1.65	0.08

AChE and BChE inhibition is expressed as the mean ± SD (n = 3 experiments). Selectivity to BChE: IC_{50} for AChE/IC_{50} for BChE. *Galantamine (Gal) was used as positive control. n.d.: not determined.

2.3. Molecular modeling studies

In order to have a better understanding of the experimental results obtained, we carried out a molecular modeling study for compounds **12**-**21**. It should be noted that calculations were carried out considering that the amino group is protonated at physiological pH. Results previously reported by our group regarding to a well-known AChE inhibitor, galantamine, was also included here for discussion [29,30]. This study was performed in three stages. First, we conducted docking calculations which led us to find the probable modes of interaction between ligands and the active site of both enzymes. Next, we performed molecular dynamics (MD) simulations with the aim of analyzing compound behavior over time. In the last stage, using the trajectories obtained from MD simulations, we calculated free energy of different complexes and carried out a per-residue analysis in order to identify the AChE and BChE active site amino acids involved in the intermolecular interactions of the different complexes. Although biological tests were performed with *Ee*AChE, the crystalline structure of *Tc*AChE

View Article Online
DOI: 10.1039/D0NJ00282H

was used in molecular modeling studies. This is possible since both enzymes are considered structurally homologous [31]. The ligand binding pockets in *Tc*AChE, *Ee*AChE and even AChE in vertebrates, have almost the same geometry, therefore, they are expected to bind inhibitors in a very similar manner [31–33].

Considering the experimental results, it should be noticed that most compounds reported here showed greater inhibitory activity against BChE than that observed against AChE. This might be due to the difference in the active sites of both enzymes. BChE active site presents a larger accessible area than the AChE active site since it has a lower number of aromatic residues in its binding pocket [34]. Both enzymes have over 60% of sequence identity and show a similar response to a number of classical inhibitors since the amino acid sequence at the active site of both AChE and BChE is well conserved [35]. Additionally, the existence of a catalytic triad (Ser, His and Glu) in the active site is considered important for the catalytic activity of both enzymes [36,37]. However, six residues, i.e. Tyr70, Tyr121, Trp279, Phe288, Phe290 and Phe330, with bulky aromatic side chains present in the AChE active site are substituted by non-aromatic residues of Asn68, Gln119, Ala277, Val286, Val288 and Ala328 in BChE. This may generate the appropriate conditions for these compounds to better accommodate in the active site of BChE.

4'-*O*-methylnorbelladine (**12**) and its halogenated derivatives at C2 (**13**-**15**) showed AChE inhibitory activity, being compound **14** one the most active of all analogues studied here. Figure 2A shows the main interactions stabilizing **14**-AChE complex. These interactions involve the following enzyme residues: Gln69, Trp84, Gly118, Ser122, Gly123, Ser124, Phe330 and Tyr334. Our simulations suggest that OH at C3 (A-ring) establishes an H-bond with the side chain of Gln69 and that OMe at C4 interacts with Ser124 backbone (Figure S1). The interactions with residues Trp84, Gly118, Ser122 and Phe330 are the same to those previously reported for galantamine [30] (Figure 2B), suggesting that these compounds are located in the same AChE region. It should be noted that activity increases when H at C2 of compound **12** is substituted by chlorine and bromine, resulting in compounds **13** and **14**, respectively. It is important to highlight that **14** is about 4 times more active than **12**. The presence of a halogen atom in norbelladine analogues allows intermolecular interactions that favorably contribute to the stability of the complexes. However, it seems that halogen atoms also play an important role from the steric point of view; compound **15** with an iodine atom showed the lowest activity of this series. These results could be related to the AChE active site size, since compounds with bulky substituents cannot accommodate properly to establish

View Article Online
DOI: 10.1039/D0NJ00282H

favorable interactions compared to the other compounds of the same series (compare inhibitory effects of compounds **13**-**15**). Figure 3 shows the histogram obtained for compound **15.** In this case significant interactions were observed for Asp72, Tyr121 and Trp279, all of them belonging to the peripheral anionic site or bottleneck region [37]. These results suggest that compound **15** is located out of the AChE active site and establishes a different interaction pattern in comparison with compounds **13** and **14**, which could explain its poor activity.

View Article Online
DOI: 10.1039/D0NJ00282H

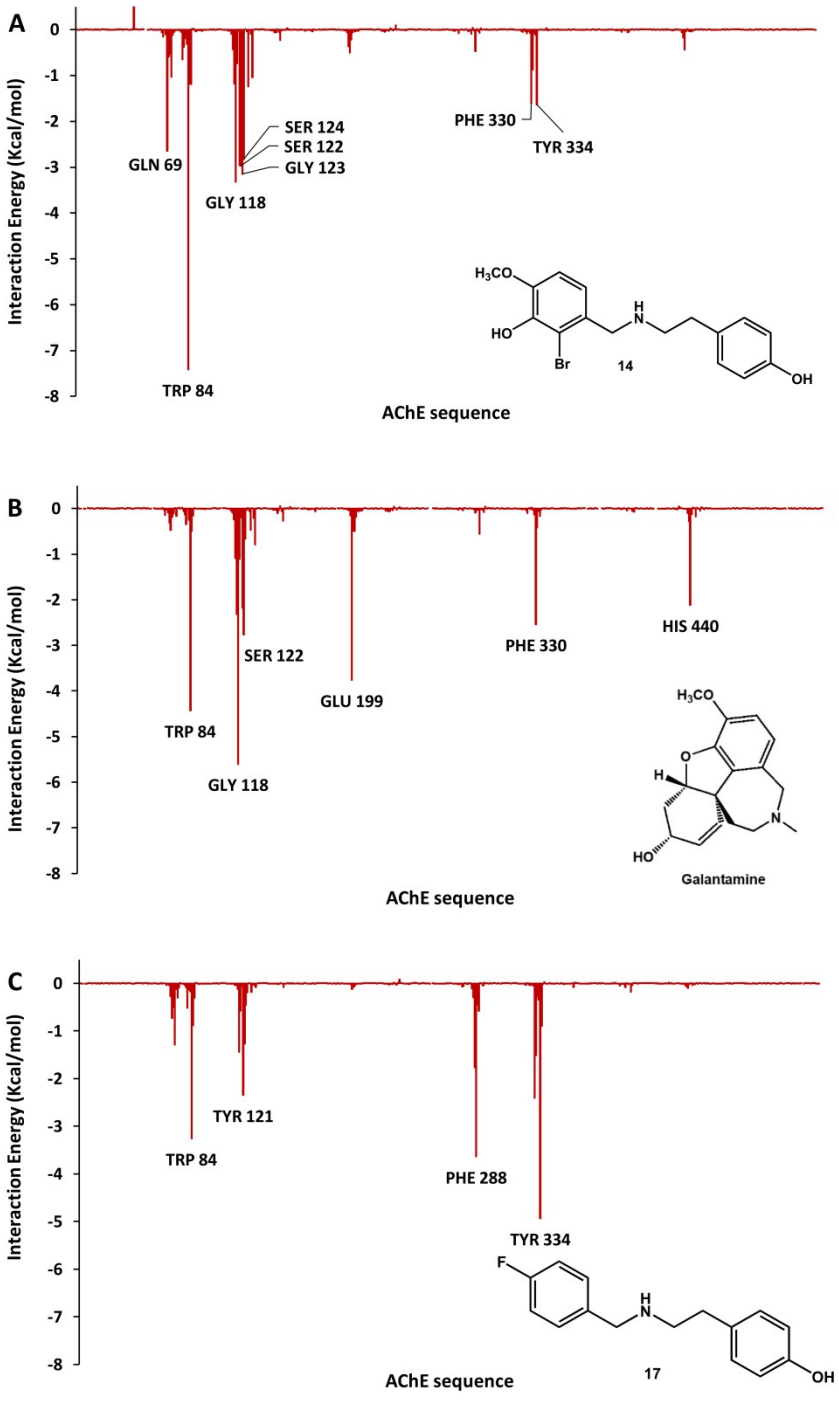

Fig. 2. Histograms of interaction energies partitioned with respect to AChE amino acid sequence when complexed with compound **14** (A), Gal (B) and compound **17** (C). The X-axis denotes the residue number of AChE and the Y-axis denotes the interaction energy between the compounds and a specific residue. Negative values and positive values are favorable or unfavorable to binding, respectively.

View Article Online
DOI: 10.1039/D0NJ00282H

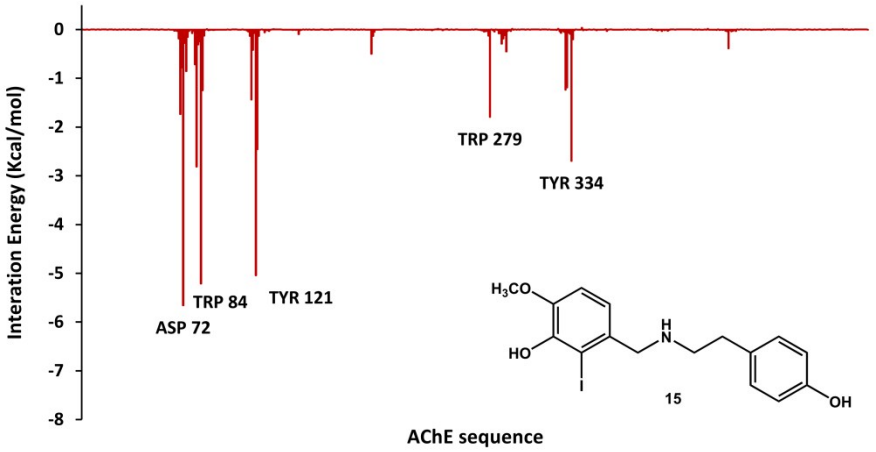

Fig. 3. Histograms of interaction energies partitioned with respect to AChE amino acid sequence when complexed with compound **15**. The X-axis denotes the residue number of AChE and the Y-axis denotes the interaction energy between the compounds and a specific residue. Negative values and positive values are favorable or unfavorable to binding, respectively.

Regarding **21**, one of the most active compounds with an IC_{50} value of 17.14 ± 3.17 μM, it is structurally very similar to **14**, being their only difference the lack of OH at B-ring. This suggests that the presence of this substituent in this position is not an important structural requirement for inhibition activity.

On the other hand, monosubstituted derivatives at the A-ring (**17**-**20**) showed IC_{50} values ≥ 200 μM for AChE, and therefore, they were considered as inactive. Figure 2C shows the histogram corresponding to **17**, as an example of these inactive compounds. It should be noted that due to the different pattern of substitutions, the important interactions with Gln69 and Ser122 discussed above are missing for this compound.

Regarding BChE, Figure 4A shows the histogram obtained for compound **15.** The main interactions stabilizing the complex are Trp110, Glu225, Phe357, and His466 among others. Similar results were obtained for the rest of the active compounds. Comparing these results with those observed for BChE-Gal complex [29] (Figure 4B), it is reasonable to assume that derivatives **12**-**21** interact with the same region of the enzyme. In all complexes, the protonated amino group of ligands is oriented towards the carboxyl group of Glu225, establishing a salt bridge in most cases (Figure S2).

View Article Online
DOI: 10.1039/D0NJ00282H

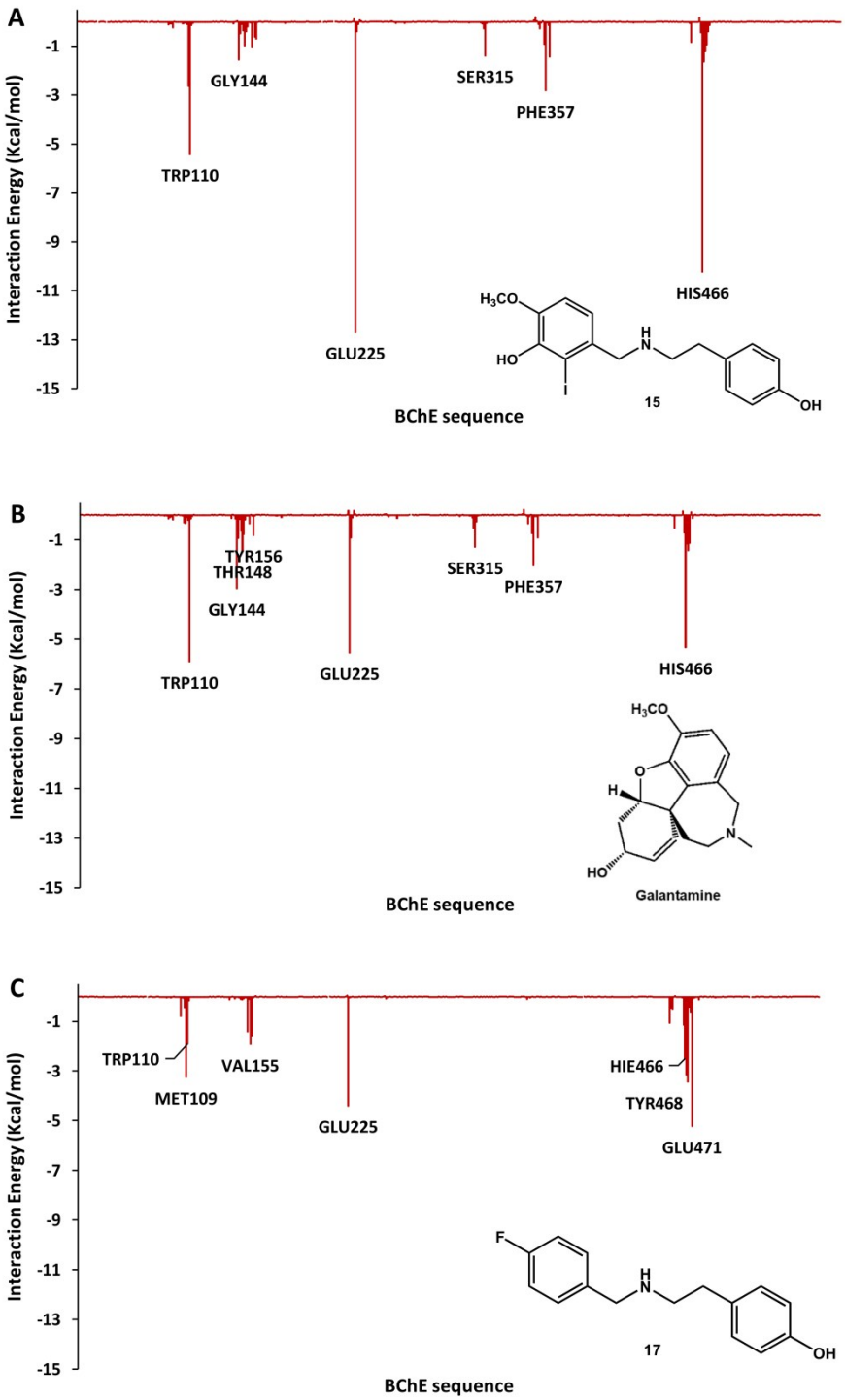

Fig. 4. Histograms of interaction energies partitioned with respect to BChE amino acid sequence when complexed with compound **15** (A), Gal (B) and compound **17** (C). The X-axis denotes the residue number of BChE and the Y-axis denotes the interaction energy between the compounds and a specific residue. Negative values and positive values are favorable or unfavorable to binding, respectively.

View Article Online
DOI: 10.1039/D0NJ00282H

On the other hand, the inhibitory effect of compounds **13** to **15** increases with the atomic radius of the halogen in position R_1. This might be due to the possibility that the iodine substituent in **15** establishes a higher number of interactions with neighboring amino acids than the rest of halogen derivatives tested. Compound **15** with IC_{50} value lower than galantamine, establishes strong interactions with Trp110, Glu225 and His466 (Figure 4A). In this line, the presence of the OH substituent at the B-ring seems to be important for this compound to show inhibitory activity since an H-bond can be formed with the backbone of Trp110 (Figure S2). It is important to notice that compound **15** is the most active against BChE in this series. However, this compound does not display significant inhibitory activity against AChE. As discussed above, the amino acid sequence in BChE active site allows to accommodate bulkier ligands if compared to AChE. Figure 5 represents the spatial view of both cholinesterases active sites when complexed with compound **15**. As can be seen, **15** adopts a different spatial arrangement in each complex. In **15**-AChE complex (Figure 5A), the ligand remains close to the surface of the active site interacting with amino acid residues from the peripheral anionic site and the bottleneck region. In contrast, in the **15**-BChE complex (Figure 5B), the ligand is located deeper in the gorge and can interact with the catalytic triad and the acyl-binding pocket of the cholinesterase.

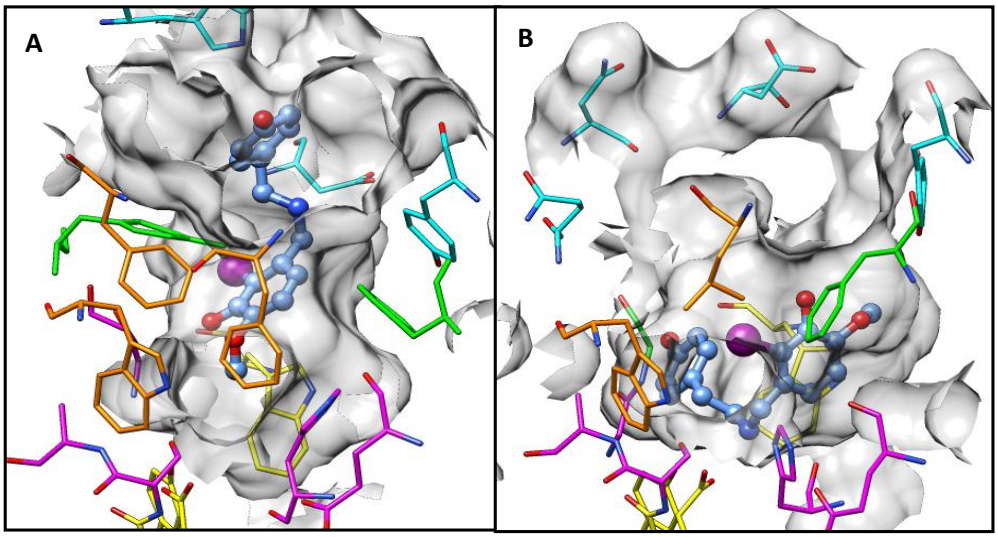

Fig. 5. Active sites of *Torpedo californica* acetylcholinesterase (AChE) (**A**) and *Equus caballus* butyrylcholinesterase (**B**) when complexed with compound **15** which is represented in ball and stick and colored in blue. The gorge of each enzyme is depicted by its molecular surface in semi-transparent gray. The main amino acid residues from both active sites are also shown. The catalytic triad and oxyanionic subsite residues are in magenta. The acyl-binding pocket amino acids are in orange. The anionic subsite is colored in yellow. The peripheral anionic site is represented in cyan. The residues from the bottle neck region are in green.

View Article Online
DOI: 10.1039/D0NJ00282H

The inactive compound **17** (IC_{50} > 200 µM) showed a different interaction pattern and interaction energy values in comparison with **15-**BChE and **21-**BChE. In Figure 4C, it can be seen that in **17**-BChE interactions with Trp110 and His466 are significantly decreased. The main interactions stabilizing the **17**-BChE complex are those with Met109, Val155, Tyr468 and Glu471.

An unexpected result was the remarkable inhibitory activity of compound **21** (IC_{50} = 13.35 ± 3.01 µM) despite the lack of the OH substituent in B-ring. Unlike **14** and **15**, in which the OH group of the phenethyl moiety establishes an H-bond with the backbone of Trp110, **21** adopts a different conformation that favors the interaction between Ser315 and OH at C3 from A-ring. Additionally, a better hydrophobic interaction with Trp110 can be observed for this compound (Figure S3). These results may explain, at least in part, the significant inhibitory activity found for compound **21**.

3. Conclusions

The synthesis of a series of *N*-benzyl-2-phenylethanamine derivatives was optimized and performed by a simple methodology involving a reductive amination affording the products with moderate to excellent yields. Most of these compounds exerted significant *in vitro* inhibition of AChE and BChE. In particular, brominated norbelladine analogues showed the highest inhibition values, whereas the presence of iodine showed a high selectivity towards BChE with a strong IC_{50} value comparable to galantamine. Moreover, the lack of hydroxyl group on the B-ring had an influence on the inhibition of BChE showing a high inhibition with similar values for both enzymes. All these observations can be explained by molecular modeling studies considering the size and structural features of the active sites of both enzymes. Due to the presence of different halogens on one of the aromatic rings, these compounds can adopt different conformations that allow some of them to accommodate very well in the active site by establishing the necessary interactions to stabilize the molecular complexes. These results can be very useful for the design and development of new inhibitors possessing similar structural characteristics.

View Article Online
DOI: 10.1039/D0NJ00282H

4. Experimental Section

4.1. General experimental procedures

4.1.1. Chemicals

3-Hydroxy-4-methoxybenzaldehyde **(1)**, 4-fluorobenzaldehyde **(6)**, 4-chlorobenzaldehyde **(7),** 4-bromobenzaldehyde **(8)**, 4-hydroxybenzaldehyde **(9),** tyramine **(10)**, phenylethylamine **(11)** were purchased from Sigma–Aldrich, Argentina. Aldehydes **2-5** were prepared by halogenation reactions. Compounds **12**-**21** were obtained by reductive amination as described in Section 4.2.3. Their NMR spectra and GC-FID or GC-MS chromatograms are shown in the Supplementary Material.

4.1.2. Analytical methods

Thin-layer chromatography (TLC) was performed on silica gel 60 F_{254} plates (Merck) using *n*-hexane:ethyl acetate mixtures of different polarity for halogenated aldehydes and diclorometane:methanol:NH_4OH (80:15:5) for norbelladine analogues and visualized by UV irradiation at 254 nm and further sprayed with acidic anisaldehyde solution. The GC-FID and GC-MS analyses were performed using a Perkin Elmer Clarus 500 and a Thermo Trace 1300 gas chromatograph coupled to an ITQ900 ion trap mass spectrometer (GC/MS-ITQ Thermo Scientific), respectively. ^{1}H and ^{13}C NMR spectra were recorded using a Bruker AC-200 spectrometer in $CDCl_3$ or D_2O at 200 and 50 MHz or Bruker Avance 400 MHz spectrometer at 400 and 100 MHz, respectively. Melting points were determined with Leitz Wetzlar 553174 (1.25 X) apparatus (Germany).

4.2. Synthesis

4.2.1. Synthesis of halogenated aldehydes

2-bromo-3-hydroxy-4-methoxybenzaldehyde **(2)**

NBS (1.75 g, 9.86 mmol) was dissolved in 60 mL of glacial acetic acid. A solution of 3-hydroxy-4-methoxybenzaldehyde (**1**) (1.5 g, 9.86 mmol) in 30 mL of glacial acetic acid, was added dropwise. The reaction mixture was stirred at room temperature for 4 h. After that the precipitated solid was filtered and washed with glacial acetic acid and then with water. Finally, the product was dried under vacuum to obtain **2** as a white solid (1.51 g, 66 % yield). Mp: 200 °C (Mp. Lit. 210 °C [38]). ^{1}H NMR (200 MHz, $CDCl_3$) δ 4.01 (s, 3H, CH_3), 6.08 (s, 1H, OH), 6.93

View Article Online
DOI: 10.1039/D0NJ00282H

(d, *J* = 8.6 Hz, 1H, Ar), 7.58 (d, *J* = 8.6 Hz, 1H, Ar), 10.26 (s, 1H, CHO). ^{13}C NMR (50 MHz, $CDCl_3$) δ 56.7, 109.4, 113.0, 122.9, 127.3, 143.3, 151.8, 191.1.

6-bromo-3-hydroxy-4-methoxybenzaldehyde **(3)**

To obtain **3** we followed the methodology described by Hazlet and Brotherton [39] with modifications. To a solution of **1** (1 g, 6.6 mmol) in 25 mL of chloroform, a solution of bromine (1.5 g, 9.5 mmol) in 10 mL of chloroform was added dropwise. The mixture was heated at 60 °C by reflux under argon atmosphere for 1 hour. The reaction was stopped in absence of starting material and evaporated to dryness. The solid was resuspended in ethyl acetate and washed with sodium thiosulfate solution (10 %) to eliminate the bromine excess. The organic phase was washed with H_2O and the aqueous phase with chloroform. Organic phases were dried and evaporated and the crude product was purified by chromatography on silica gel (70–230 mesh, Sigma-Aldrich) with dichloromethane to afford a pale brown solid (1.1 g, 73 % yield). Mp: 118-120 °C (Mp. Lit. 112-114°C. [40]). ^{1}H NMR (200 MHz, $CDCl_3$) δ 3.99 (s, 3H, CH_3), 5.63 (s, 1H, OH), 7.06 (s, 1H, Ar), 7.48 (s, 1 H, Ar), 10.18 (s, H, CHO). ^{13}C NMR (100 MHz, $CDCl_3$) δ 56.6, 114.6, 115.1, 118.7, 127.4, 145.4, 151.9, 190.8.

2-chloro-3-hydroxy-4-methoxybenzaldehyde **(4)**

To a solution of 3-hydroxy-4-methoxybenzaldehyde (**1**) (1.5 g, 9.86 mmol) in 30 mL of glacial acetic acid, was added dropwise a solution of NCS (1.97 g, 14.8 mmol) in 60 mL of glacial acetic acid. The reaction was carried out for 24 h. The precipitated solid formed was filtered and washed with glacial acetic acid and water to yield **4**. The resulting product was a white solid (582 mg, 48 % yield). Mp: 187-189 °C. ^{1}H NMR (200 MHz, $CDCl_3$) δ 4.01 (s, 3H, CH_3), 5.97 (s, 1H, OH), 6.90 (d, 1H, *J* = 8.6 Hz, Ar), 7.57 (d, 1H, *J* = 8.6 Hz, Ar), 10.35 (s, 1H, CHO). ^{13}C NMR (50 MHz, $CDCl_3$) δ 56.7, 108.9, 122.2, 123.2, 126.5, 142.3, 152, 189.1.

3-hydroxy-2-iodo-4-methoxybenzaldehyde **(5)**

The iodination of 3-hydroxy-4-methoxybenzaldehyde was obtained according to literature [41] with modifications. 3-Hydroxy-4-methoxybenzaldehyde (1.5 g, 9.86 mmol) and NaI (1.73 g, 11.53 mmol) was dissolved in EtOH (30 mL). NaClO (16.4 mL, 9.86 mmol) was added dropwise to the solution. The precipitate formed was filtered and washed with cold water. The ocher solid was obtained in 46 % yield. Mp: 170-172 °C. ^{1}H NMR (200 MHz, $CDCl_3$-DMSO-*d6*) δ 4.00 (s, 3H, CH_3), 6.93 (d, 1H, *J* = 8.5 Hz, Ar), 7.56 (d, 1H, *J* = 8.5 Hz, Ar), 10.04 (s, 1H, CHO). ^{13}C NMR (50 MHz, $CDCl_3$) δ 56.7, 88.2, 110.1, 124.0, 128.8, 145.8, 150.8, 194.9.

View Article Online
DOI: 10.1039/D0NJ00282H

4.2.3. General procedure for the synthesis of N-benzyl-2-phenylethanamines (**12-21**)

To obtain the norbelladine analogues, we followed the procedure described by Tachy *et al.* [26] with modifications. Aldehydes **1-9** (2.16 mmol) and amines **10-11** (2.16 mmol) were dissolved in MeOH (12 mL) and anhydride Na_2SO_4 and triethylamine (TEA) (400 µL) or KOH (100 mg) were added. The reaction was stirred overnight under inert atmosphere. After that, the imine formed was reduced with $NaBH_4$ (2.16 mmol) on ice bath until no starting material was observed by TLC. The solvent was evaporated and the solid was resuspended in water. The pH of the aqueous phase was adjusted to the corresponding theoretical isoelectric point of the products. The precipitated product was filtered and dried under vacuum. The solid was dissolved in hot ethanol and after cooling, the suspension was filtered. The resulting solid was dried to yield the desired product. To obtain the corresponding hydrochloride, each compound was dissolved in absolute EtOH and then HCl was added in equimolar relation with the product. The reaction was stirred for 3 h and after that, the solvent was evaporated and the residue washed with acetone.

N-(p-hydroxyphenylethyl)-N-(3-hydroxy-4-methoxy)benzylamine **(12)** beige solid. 51 % yield. Mp: 206-208 °C (Mp. Lit. 208° [26]). ^{1}H NMR (200 MHz, D_2O) as hydrochloride: δ 2.92 (m, 2H, CH_2), 3.25 (m, 2H, CH_2), 3.88 (s, 3H, OCH_3), 4.11 (s, 2H, CH_2), 6.85-7.18 (m, 7H, Ar). ^{13}C NMR (50 MHz) 30.5, 47.5, 50.2, 55.7, 112.4, 115.6, 116.5, 122.5, 123.2, 128.0, 130.0, 144.9, 148.2, 154.4.

N-(p-hydroxyphenylethyl)-N-(2-chloro-3-hydroxy-4-methoxy)benzylamine **(13)** Light brown solid. 66 % yield. Mp: 172 °C. ^{1}H NMR (200 MHz, $CDCl_3$) δ 2.72-2.82 (m, 4H, CH_2-CH_2), 3.82 (s, 2H, CH_2), 3.87 (s, 3H, OCH_3), 6.69-6.82 (m, 4H, Ar), 7.00 (d, *J* = 8.4 Hz, 2H, Ar). ^{13}C NMR (100 MHz, D_2O) as hydrochloride: δ 30.5, 47.9, 48.2, 56.2, 110.3, 115.7, 120.7, 121.0, 123.4, 128.0, 130.1, 142.0, 149.5, 154.6.

N-(p-hydroxyphenylethyl)-N-(2-bromo-3-hydroxy-4-methoxy)benzylamine **(14)** light brown solid. 77 % yield. Mp: 185-187 °C. ^{1}H NMR (200 MHz, $CDCl_3$) δ 2.75-2.85 (m, 4H, CH_2-CH_2), 3.83 (s, 2H, CH_2), 3.87 (s, 3H, OCH_3), 6.67-6.86 (m, 4H, Ar), 7.02 (d, *J* = 8.3, 2H, Ar). ^{13}C NMR (100 MHz, D_2O) as hydrochloride: 30.4, 47.8, 50.9, 56.1, 110.7, 111.4, 115.6, 122.4, 123.5, 127.8, 130.0, 143.0, 149.0, 154.4.

View Article Online
DOI: 10.1039/D0NJ00282H

N-(p-hydroxyphenylethyl)-N-(2-iodo-3-hydroxy-4-methoxy)benzylamine **(15)** Ocher solid 49 % yield. Mp: 202-205 °C (as hydrochloride). ^{1}H NMR (400 MHz, D_2O) as hydrochloride δ 2.93-3.36 (m, 4H, CH_2-CH_2), 3.87 (s, 2H, CH_2), 4.32 (s, 3H, OCH_3), 6.84 (d, *J* = 8.2 Hz, 2H, Ar), 7.02 (s, 2H, Ar), 7.15 (d, *J* = 8.2 Hz, 2H, Ar). ^{13}C NMR (100 MHz, D_2O) δ 30.6, 48.0, 54.9, 56.2, 89.4, 111.7, 115.8, 123.5, 126.0, 127.9, 130.1, 145.8, 147.8, 154.6.

N-(p-hydroxyphenylethyl)-N-(6-bromo-3-hydroxy-4-methoxy)benzylamine **(16)** Pale yellow solid. 56 % yield. Mp: 122-125 °C. ^{1}H NMR (200 MHz, $CDCl_3$) δ 2.75- 2.84 (m, 4H, CH_2-CH_2), 3.75 (s, 2H, CH_2), 3.85 (s, 3H, OCH_3), 6.73 (d, *J* = 8.4 Hz, 2H, Ar), 6.88 (s, 1H, Ar), 6.96 (s, 1H, Ar), 7.05 (d, *J* = 8.4 Hz, 2H, Ar). ^{13}C NMR (100 MHz, $CDCl_3$) δ 35.4, 50.3, 53.1, 56.2, 112.6, 115.0, 115.3, 116.2, 129.8, 132.1, 144.9, 146.1, 153.8.

N-(p-hydroxyphenylethyl)-N-(p-fluor)benzylamine **(17)** yellow solid. 51 % yield. Mp: 163-165 °C. ^{1}H NMR (400 MHz, D_2O) as hydrochloride δ 2.91-3.28 (m, 4H, CH_2-CH_2), 4.20 (s, 2H, CH_2), 6.87 (d, 2H, Ar), 7.15-7.21 (m, 4H, Ar), 7.42-7.46 (m, 2H, Ar). ^{13}C NMR (200 MHz, D_2O) δ 30.7, 47.9, 50.2, 115.8, 116.0, 116.2, 126.6, 128.2, 130.2, 132.0, 132.1, 154.6, 162.0, 164.4.

N-(p-hydroxyphenylethyl)-N-(p-chloro)benzylamine **(18)** pale yellow solid. 55 % yield. Mp: 123-126 °C. ^{1}H NMR (400 MHz, D_2O) as hydrochloride δ 2.91- 3.28 (m, 4H, CH_2-CH_2) 4.20 (s, 2H, CH_2), 6.87 (d, *J* = 8.4 Hz, 2H, Ar), 7.16 (d, *J* = 8.3, 2H, Ar), 7.39 (d, *J* = 8.4, 2H, Ar), 7.46 (d, *J* = 8.4, 2H, Ar). ^{13}C NMR (100 MHz, $CDCl_3$) δ 30.6, 47.9, 50.1, 115.7, 128.1, 129.1, 129.2, 130.1, 131.3, 135.0, 154.5.

N-(p-hydroxyphenylethyl)-N-(p-bromo)benzylamine **(19)** white solid. 84 % yield. Mp: 140-143 °C. ^{1}H NMR (200 MHz, $CDCl_3$) δ 2.75-2.84 (m, 4H, CH_2-CH_2), 3.75 (s, 2H, CH_2), 6.73 (d, *J* = 8.3 Hz, 2H, Ar), 7.04 (d, *J* = 8.3 Hz, 2H, Ar), 7.15 (d, *J* = 8.2 Hz, 2H, Ar), 7.42 (d, *J* = 8.2 Hz, 2H, Ar). ^{13}C NMR (100 MHz, $CDCl_3$) δ 35.2, 50.5, 53.2, 115.6, 121.0, 129.9, 130.1, 131.4, 131.7, 138.8, 154.6.

N-(p-hydroxyphenylethyl)-N-(p-hydroxy)benzylamine **(20)** white solid. 92 % yield. Mp: 220-222 °C (as hydrochloride). ^{1}H NMR (400 MHz, D_2O) as hydrochloride δ 2.87-3.23 (m, 4H, CH_2-CH_2), 4.11 (s, 2H, CH_2), 6.84 (d, *J* = 8.5 Hz, 2H, Ar), 6.90 (d, *J* = 8.5, 2H, Ar), 7.13 (d, *J* = 8.5 Hz, 2H, Ar), 7.28 (d, *J* = 8.5 Hz, 2H, Ar). ^{13}C NMR (100 MHz, D_2O) δ 30.6, 47.6, 50.3, 115.8, 122.3, 128.2, 130.1, 131.6, 154.5, 156.5.

N-(phenylethyl)-N-(2-bromo-3-hydroxy-4-methoxy)benzylamine **(21)** pale yellow solid. 55 % yield. Mp: 102-105 °C. ^{1}H NMR (400 MHz, $CDCl_3$) 2.85-2.96 (m, 4H, CH_2CH_2), 3.89 (s, 3H,

View Article Online
DOI: 10.1039/D0NJ00282H

OCH$_3$), 3.91 (s, 2H, CH$_2$), 6.76 (d, *J* = 8.3 Hz, 1H, Ar), 6.88 (d, *J* = 8.3 Hz, 1H, Ar), 7.18-7.30 (m, 5H, Ar). ^{13}C NMR (100 MHz, CDCl$_3$) δ 35.2, 49.2, 52.4, 56.3, 109.4, 110.3, 121.5, 126.4, 128.6, 128.7, 138.9, 143.3, 146.6.

4.3. Microplate assay for AChE and BChE inhibitory activities

The enzymes AChE from *Electrophorus electricus* (*Ee*AChE) and BChE from equine serum (*Eq*BChE) (Sigma-Aldrich) were used. For the AChE and BChE activity assay, acetylthiocholine iodide and butyrylthiocholine iodide were used as substrates, respectively. Briefly, 50 µL of AChE or BChE in phosphate-buffered saline (PBS) (8 mM K_2HPO_4, 2.3 mM NaH_2PO_4, 0.15 M NaCl, pH 7.6) and 50 µL of the sample dissolved in the same buffer, were added to the wells of a microplate. When necessary, the compounds were dissolved in dimethyl sulfoxide (DMSO) or methanol at a final concentration of 0.02 % and 0.5 %, respectively The plates were incubated for 30 min at room temperature before the addition of 100 µL of the substrate solution (0.1 M Na_2HPO_4, 0.5 M DTNB, 0.6 mM ATCI in Millipore water, pH 7.5). The absorbance was read in a Thermo Scientific Multiskan FC microplate photometer at 405 nm after 5 min. Enzyme inhibitory activity was calculated as a percentage compared to an assay using buffer without any inhibitor. The results obtained were analyzed with the software package Prism (Graph Pad Inc., San Diego, CA, USA). The values were expressed as half-maximal inhibitory concentration IC_{50} (µM), and were calculated as means ± SD of 3 individual determinations. Galantamine (Sigma-Aldrich) was used as a positive control.

4.4. Molecular Modeling Studies

3D models of *Torpedo californica* AChE (*Tc*AChE) (1DX6) [42] and *Equus caballus* BChE (*Eq*BChE) (UniProtAC Q9N1N9) available at Protein Data Bank (http://www.rcsb.org) were used for carring out the molecular modeling studies. Water molecules and ligands were removed from the structures before performing the docking calculations. Receptors and *N*-benzyl-2-phenylethanamine derivatives structures were converted from pdb to pdbqt format using AutoDockTools 1.5.4 [43]. Gasteiger charges were added for all the compounds and non-polar hydrogen atoms were merged. AutoDockTools [43] was also used to perform further graphic manipulations and visualizations required. For docking procedures, Autodock version

View Article Online
DOI: 10.1039/D0NJ00282H

4.0 [44] was used. The receptor structure was set as rigid and grid dimension were 60 60 60 for the X, Y and Z axes, respectively, in the catalytic site of *Tc*AChE and *Eq*BChE with a spacing resolution of 0.375 Å in both cases. All torsions of the ligand were allowed to rotate during docking. The number of collected poses was 200. Other parameters were set to default values. The resulting docked conformations were clustered into families based on the rmsd between the coordinates of the ligands and were ranked regarding to the binding free energy of complexes. The structure with lower binding free energy from the cluster with the largest number of members was chosen as the optimum docking conformation and was used in subsequent simulations.

MD simulations for all complexes selected from docking procedures were performed using the Amber16 software package [45]. Antechamber software [46] was used to generate their parameters with FF99SB [47] and GAFF [48] force fields. The complex geometries from docking were soaked in truncated octahedral periodic boxes of explicit water using the TIP3P model [49] with a margin of 10.0 Å in each direction from the solute. Na^+ or Cl^- ions were placed by Leap to neutralize the negative and positive charges of AChE and BChE complexes, respectively. The energy of each system was then minimized with sander module using a steepest-descent algorithm for 1000 steps. There upon the complexes were equilibrated during 500 ps at constant volume. The SHAKE algorithm [50] was applied allowing for an integration time step of 2 fs. The systems were heated from 0 to 300 K using Langevin thermostat [51] in order to control temperature, collision frequency = 1.0 ps^{-1}. Next, three MD simulations were conducted for each complex at 298 K target temperature. All production was performed under NVT conditions. The particle mesh Ewald (PME) method [52] was applied using a grid spacing of 1.2 Å, a spline interpolation order of 4, and a real space direct sum cutoff of 8.0 Å. Simulation time was set to 20 ns, the time step was set to 2.0 fs and coordinates were saved for analysis every 10 ps. Post MD analysis was performed with the program PTRAJ [53]. A per-residue interaction energy decomposition analysis using mm_pbsa program was carried out in order to determine the residues of AChE and BChE that interact with each ligand. For mm_pbsa methodology [54], snapshots from the corresponding last 1000 ps of MD trajectories were considered. The explicit water molecules and counter ions were removed from the snapshots.

Declaration of Competing Interest

There are no conflicts to declare.

View Article Online
DOI: 10.1039/D0NJ00282H

Acknowledgments

The manuscript was written through contributions of all authors. Authors thank Lic. Mónica Ferrari for technical assistance and Dr. Walter Stege for NMR spectra. Funding: This work was supported by grants from UNSL (PROICO 2-1716), CONICET (PIP 1122015 0100090) and ANPCyT (PICT 2018-02916, PICT 2014-03425 and PICT 2015-1769), CICITCA UNSJ. F.C.V. and D.Z.P. are doctoral CONICET fellows; M.K.S, G.E.F., D.E., O.P., A.G. and A.A.O are members of the Research Career of CONICET.

Appendix A. Supplementary material

Supplementary data associated with this article can be found in the online version.

References

1 J. F. González, A. R. Alcántara, A. L. Doadrio and J. M. Sánchez-Montero, *Expert Opin. Drug Discov.*, 2019, **14**, 879–891.

2 K. Sharma, *Mol. Med. Rep.*, 2019, **20**, 1479–1487.

3 A. Bosak, A. Ramić, T. Smidlehner, T. Hrenar, I. Primozic and Z. Kovaric, *PLoS One*, 2018, 1–18.

4 I. Doytchinova, M. Atanasova, I. Valkova, G. Stavrakov, I. Philipova, Z. Zhivkova, D. Zheleva-dimitrova, I. Dimitrov, I. Doytchinova, M. Atanasova, I. Valkova and G. Stavrakov, *J. Enzyme Inhib. Med. Chem.*, 2018, **33**, 768–776.

5 A. Nordberg, C. Ballard, R. Bullock, T. Darreh-Shori and M. Somogyi, *Prim. Care Companion CNS Disord.*, 2013, **15**, 1–11.

6 T. C. dos Santos, T. M. Gomes, B. A. S. Pinto, A. L. Camara and A. M. de A. Paes, *Front. Pharmacol.*, 2018, **9**, 1192.

7 M. S. Shah, S. U. Khan, S. A. Ejaz, S. Afridi, S. U. F. Rizvi, M. Najam-ul-Haq and J.

View Article Online
DOI: 10.1039/D0NJ00282H

Iqbal, *Biochem. Biophys. Res. Commun.*, 2017, **482**, 615–624.

8 D. G. T. Parambi, F. Aljoufi, V. Murugaiyah, G. E. Mathew, S. Dev, B. Lakshminarayanan, O. M. Hendawy and B. Mathew, *Cent. Nerv. Syst. Agents Med. Chem.*, 2019, **19**, 67–71.

9 Z. Sang, K. Wang, J. Shi, W. Liu and Z. Tan, *Eur. J. Med. Chem.*, 2019, **178**, 726–739.

10 A. Rastegari, H. Nadri, M. Mahdavi, A. Moradi, S. S. Mirfazli, N. Edraki, F. H. Moghadam, B. Larijani, T. Akbarzadeh and M. Saeedi, *Bioorg. Chem.*, 2019, **83**, 391–401.

11 X. Kou, L. Song, Y. Wang, Q. Yu, H. Ju, A. Yang and R. Shen, *Bioorg. Med. Chem. Lett.*, 2020, **30**, 126927.

12 G. L. Delogu, M. J. Matos, M. Fanti, B. Era, R. Medda, E. Pieroni, A. Fais, A. Kumar and F. Pintus, *Bioorg. Med. Chem. Lett.*, 2016, **26**, 2308–2313.

13 Y. Huang, W. Min, Q.-W. Wu, J. Sun, D.-H. Shi and C.-G. Yan, *New J. Chem.*, 2018, **42**, 16211–16216.

14 J. Zhu, H. Yang, Y. Chen, H. Lin, Q. Li, J. Mo, Y. Bian, Y. Pei and H. Sun, *J. Enzyme Inhib. Med. Chem.*, 2018, **33**, 496–506.

15 J. Mo, H. Yang, T. Chen, Q. Li, H. Lin, F. Feng, W. Liu, W. Qu, Q. Guo, H. Chi, Y. Chen and H. Sun, *Bioorg. Chem.*, 2019, **93**, 103310.

16 G. F. dos Santos, G. da Silva Lima, G. Pereira de Oliveira, J. D. de Souza Filho, L. da Silva Amaral, E. Rodrigues-Filho and J. A. Takahashi, *Bioorg. Chem.*, 2018, **79**, 60–63.

17 M. B. Kilgore, M. M. Augustin, C. M. Starks, M. O'Neil-Johnson, G. D. May, J. A. Crow and T. M. Kutchan, *PLoS One*, , DOI:10.1371/journal.pone.0103223., 2014, **9**.

18 M. B. Kilgore and T. M. Kutchan, *Phytochem. Rev.*, 2016, **15**, 317–337.

19 T. Hotchandani and I. Desgagne-Penix, *Curr. Top. Med. Chem.*, 2016, **17**, 418–427.

20 J. B. Park, *Bioorganic Med. Chem. Lett.*, 2014, **24**, 5381–5384.

21 M. Hernandes, S. M. Cavalcanti, D. R. Moreira, W. de Azevedo Junior and A. C. Leite,

View Article Online
DOI: 10.1039/D0NJ00282H

Curr. Drug Targets, 2010, **11**, 303–314.

22 D. Ioffe and A. Kampf, in *Kirk-Othmer Encyclopedia of Chemical Technology*, John Wiley & Sons, Inc., Hoboken, NJ, USA, 2002.

23 Alasdair H Neilson, *Organic bromine and iodine compounds.*, Springer, Berlin, Heidelberg, 2003.

24 J. Szewczyk, A. H. Lewin and F. I. Carroll, *J. Heterocycl. Chem.*, 1988, **25**, 1809–1811.

25 F. Tozzi, S. Ley, M. Kitching and I. Baxendale, *Synlett*, 2010, **2010**, 1919–1922.

26 A. El Tahchy, M. Boisbrun, A. Ptak, F. Dupire, F. Chrétien, M. Henry, Y. Chapleur and D. Laurain-Mattar, *Acta Biochim. Pol.*, 2010, **57**, 75–82.

27 S. Saliba, A. Ptak, M. Boisbrun, R. Spina, F. Dupire and D. Laurain-Mattar, *Eng. Life Sci.*, 2016, **16**, 731–739.

28 G. L. Ellman, K. D. Courtney, V. Andres and R. M. Featherstone, *Biochem. Pharmacol.*, 1961, **7**, 88–95.

29 J. E. Ortiz, N. B. Pigni, S. A. Andujar, G. Roitman, F. D. Suvire, R. D. Enriz, A. Tapia, J. Bastida and G. E. Feresin, *J. Nat. Prod.*, 2016, **79**, 1241–1248.

30 J. E. Ortiz, A. Garro, N. B. Pigni, M. B. Agüero, G. Roitman, A. Slanis, R. D. Enriz, G. E. Feresin, J. Bastida and A. Tapia, *Phytomedicine*, 2018, **39**, 66–74.

31 H. R. Adhami, T. Linder, H. Kaehlig, D. Schuster, M. Zehl and L. Krenn, *J. Ethnopharmacol.*, 2012, **139**, 142–148.

32 S. Bon, M. Vigny and J. Massoulie, *Proc. Natil. Acad. Scn. USA*, 1979, **76**, 2546–2550.

33 H. Dvir, I. Silman, M. Harel, T. L. Rosenberry and J. L. Sussman, *Chem. Biol. Interact.*, 2010, **187**, 10–22.

34 M. Eslami, S. M. Hashemianzadeh, K. G. Moghaddam, A. Khorsandi-Lagol and S. A. Seyed Sajadi, *RSC Adv.*, 2015, **5**, 66840–66851.

35 A. S. Balasubramanian and C. D. Bhanumathy, *FASEB J.*, 1993, **7**, 1354–1358.

36 G. Gibney, S. Camp, M. Dionne, K. Macphee-Quigley and P. Taylor, *Proc. Natl. Acad.*

View Article Online
DOI: 10.1039/D0NJ00282H

Sci. U. S. A., 1990, **87**, 7551–7554.

37 J. L. Sussman, M. Harel, F. Frolow, C. Oefner, A. Goldman, L. Toker and I. Silman, *Science*, 1991, **253**, 872–9.

38 J. Maresh, A. Ralko, T. Speltz, J. Burke, C. Murphy, Z. Gaskell, J. Girel, E. Terranova, C. Richtscheidt and M. Krzeszowiec, *Synlett*, 2014, **25**, 2891–2894.

39 S. E. Hazlet and R. J. Brotherton, *J. Org. Chem.*, 1962, **27**, 3253–3256.

40 T. A. Henry and T. M. Sharp, 1930, 2279–2289.

41 G. L. Succaw and K. M. Doxsee, *Educ. Química*, 2009, **20**, 433–440.

42 H. M. Greenblatt, G. Kryger, T. Lewis, I. Silman and J. L. Sussman, *FEBS Lett.*, 1999, **463**, 321–326.

43 M. F. Sanner, *J Mol Graph Model*, 1999, **17**, 57–61.

44 G. M. Morris, R. Huey, W. Lindstrom, M. F. Sanner, R. K. Belew, D. S. Goodsell and A. J. Olson, *J. Comput. Chem.*, 2009, **30**, 2785–2791.

45 D. A. Case, R. M. Betz, D. S. Cerutti, T. E. Cheatham, III, T. A. Darden, R. E. Duke, T. J. Giese, H. Gohlke, A. W. Goetz, N. Homeyer, S. Izadi, P. Janowski, J. Kaus, A. Kovalenko, T. S. Lee, S. LeGrand, P. Li, C. Lin, T. Luchko, R. Luo, B. Madej, D. Mermelstein, K. M. Merz, G. Monard, H. Nguyen, H. T. Nguyen, I. Omelyan, A. Onufriev, D. R. Roe, A. Roitberg, C. Sagui, C. L. Simmerling, W. M. Botello-Smith, J. Swails, R. C. Walker, J. Wang, R. M. Wolf, X. Wu, L. Xiao and P. A. Kollman, *Univ. California, San Francisco,* 2016.

46 J. Wang, W. Wang, P. A. Kollman and D. A. Case, *J. Mol. Graph. Model.*, 2006, **25**, 247–260.

47 K. Lindorff-Larsen, S. Piana, K. Palmo, P. Maragakis, J. L. Klepeis, R. O. Dror and D. E. Shaw, *Proteins Struct. Funct. Bioinforma.*, 2010, **78**.

48 J. Wang, R. M. Wolf, J. W. Caldwell, P. A. Kollman and D. A. Case, *J. Comput. Chem.*, 2004, **25**, 1157–1174.

49 W. L. Jorgensen, J. Chandrasekhar, J. D. Madura, R. W. Impey and M. L. Klein, *J.*

View Article Online
DOI: 10.1039/D0NJ00282H

Chem. Phys., 1983, **79**, 926–935.

50 J.-P. Ryckaert, G. Ciccotti and H. J. C. Berendsen, *J. Comput. Phys.*, 1977, **23**, 327–341.

51 J. A. Izaguirre, D. P. Catarello, J. M. Wozniak and R. D. Skeel, *J. Chem. Phys.*, 2001, **114**, 2090–2098.

52 T. Darden, D. York and L. Pedersen, *J. Chem. Phys.*, 1993, **98**, 10089–10092.

53 D. A. Case, T. E. Cheatham, T. Darden, H. Gohlke, R. Luo, K. M. Merz, A. Onufriev, C. Simmerling, B. Wang and R. J. Woods, *J. Comput. Chem.*, 2005, **26**, 1668–1688.

54 S. Genheden and U. Ryde, *Expert Opin. Drug Discov.*, 2015, **10**, 449–461.